# Cold-formed stainless steel RHSs/SHSs under combined compression and cyclic bending

**Cheng Fang, Feng Zhou & Chenhao Luo**

Tongji University
Department of Structural Engineering
Cheng FANG, Feng ZHOU, Chenhao LUO

# OUTLINE

- BACKGROUND
- EXPERIMENTAL STUDY
- NUMERICAL INVESTIGATION
- DESIGN
- CONCLUSIONS

# BACKGROUND

- **Stainless steel has been used as construction material for both structural and architectural applications.**

**REGIONAL PARLIAMENT**
**in Belgium**
**Stainless steel 304**

**A Walk to Remember**
**in Australia**
**Stainless steel 316L**

**The KELPIES**
**in Scotland**
**Stainless steel 316L**

# BACKGROUND

- So far, most of the relevant studies focused on the behavior of stainless steel members under <u>static loading</u> conditions; however, information on their <u>seismic performance</u> is limited, which hinders a confident use of stainless steel members in seismic-active regions.

- The current study aims to investigate the structural behavior of stainless steel RHSs/SHSs under cyclic loading.

# Experimental study—Test specimens

- A total of 10 specimens were tested under constant axial load and cyclically increased uniaxial bending.
- A nominal total length (L) of 660mm is designed such that local buckling failure mode govern.

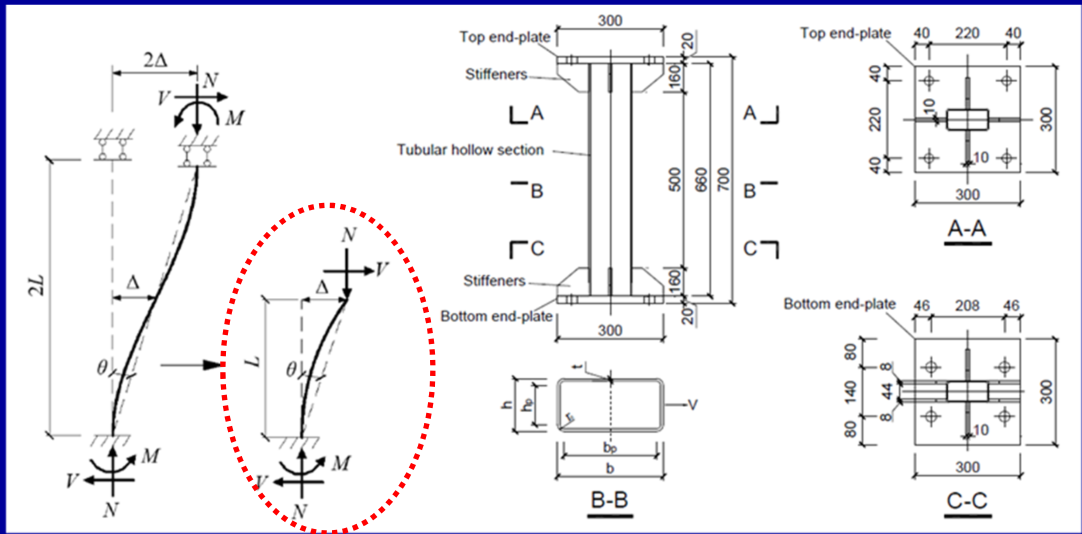


- Three tubes were selected, namely, SHS 120×120×3, RHS 120×60×3, and RHS 120×60×2, which are abbreviated as S1, R1, and R2 sections, respectively.
- The tubes were cold-rolled from Grade 304 Austenite stainless steel.

# Experimental study—Test specimens

- The test parameters cover a variety of ***section slenderness***, ***axial load ratio***, and ***bending direction***.

| Specimens | $b$ (mm) | $h$ (mm) | $t$ (mm) | $r_0$(mm) | $r_f$ | $r_w$ | $n$ | Bending direction |
|---|---|---|---|---|---|---|---|---|
| S1-n0.2 | 120.52 | 120.24 | 2.81 | 7.03 | 50.1 | 50.3 | 0.20 | - |
| S1-n0.4 | 120.52 | 120.24 | 2.81 | 7.03 | 50.1 | 50.3 | 0.40 | - |
| R1-n0.2-S | 120.29 | 61.00 | 2.72 | 6.80 | 24.7 | 55.6 | 0.20 | Strong-axis |
| R1-n0.4-S | 120.29 | 61.00 | 2.72 | 6.80 | 24.7 | 55.6 | 0.40 | Strong-axis |
| R2-n0.2-S | 120.21 | 60.37 | 1.80 | 4.51 | 39.4 | 85.4 | 0.20 | Strong-axis |
| R2-n0.4-S | 120.21 | 60.37 | 1.80 | 4.51 | 39.4 | 85.4 | 0.40 | Strong-axis |
| R1-n0.2-W | 61.00 | 120.29 | 2.72 | 6.80 | 55.6 | 24.7 | 0.20 | Weak-axis |
| R1-n0.4-W | 61.00 | 120.29 | 2.72 | 6.80 | 55.6 | 24.7 | 0.40 | Weak-axis |
| R2-n0.2-W | 60.37 | 120.21 | 1.80 | 4.51 | 85.4 | 39.4 | 0.20 | Weak-axis |
| R2-n0.4-W | 60.37 | 120.21 | 1.80 | 4.51 | 85.4 | 39.4 | 0.40 | Weak-axis |

$r_f = h_p/\varepsilon t$

$r_w = b_p/\varepsilon t$

$n = P/\sigma_{0.2}A$

| Section | $E_0$ (GPa) | $\sigma_{0.2}$ (MPa) | $\sigma_u$ (MPa) | $\varepsilon_f$ (%) | $n_f$ |
|---|---|---|---|---|---|
| S1 | 188.5 | 371.2 | 851.7 | 64.6 | 5.51 |
| R1 | 189.9 | 426.2 | 875.1 | 55.6 | 5.01 |
| R2 | 190.5 | 407.7 | 915.7 | 63.7 | 5.56 |

**Material properties**

# Experimental study—Test setup

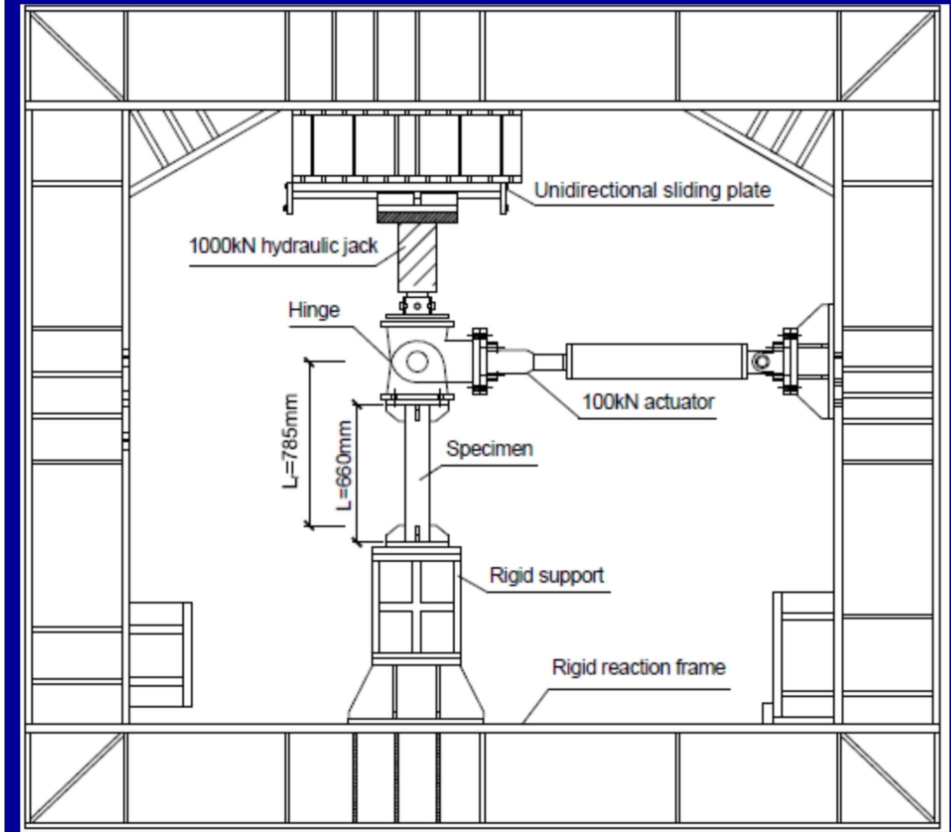


## Test instrumentation

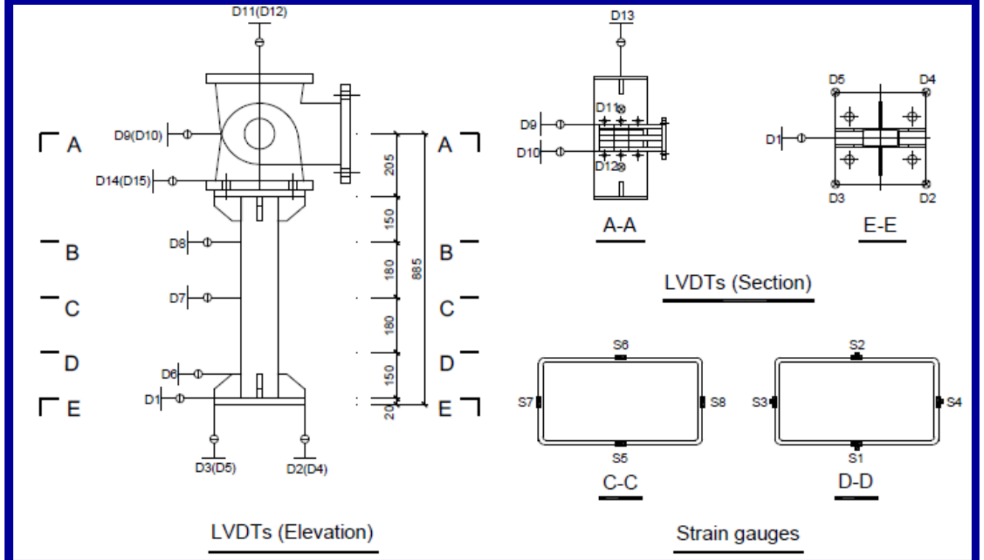


- The specimen acted as a cantilever column with a fixed bottom end and a moveable top end.
- The axial load was first applied and then maintained constant. The cyclic lateral load was subsequently applied adopting drift angle as the controlling parameter.

# Experimental study—Failure mode

- Local buckling was the governing failure mode for all the specimens.
- For the specimens with 2 mm-thick tube walls, local buckling was found at a very early stage, i.e. 0.375% - 0.5% drifts, whereas for the stockier sections (3mm-thick tubes), local buckling normally occurred beyond 1% drift.
- A decrease of the axial load ratio could evidently postpone the initiation of local buckling.




# Experimental study—Moment-drift responses (1)

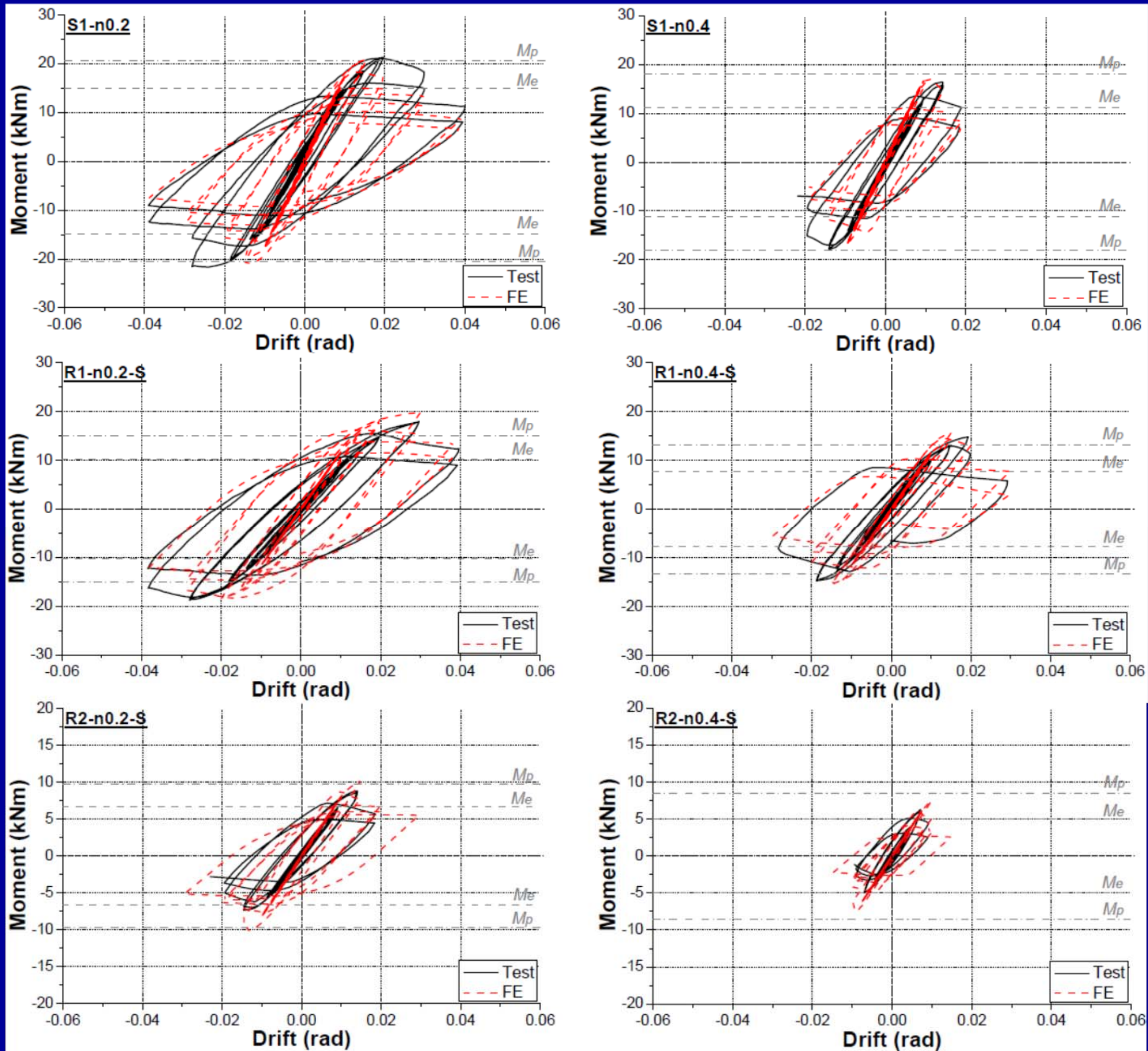


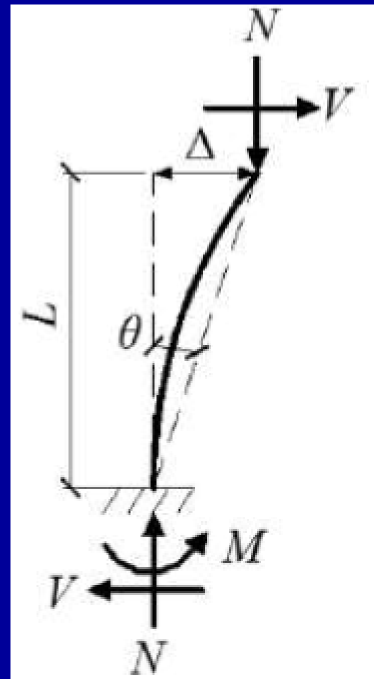


Moment, $M = VL + N\Delta$

Drift, $\theta = VL + N\Delta$

# Experimental study—Moment-drift responses(2)

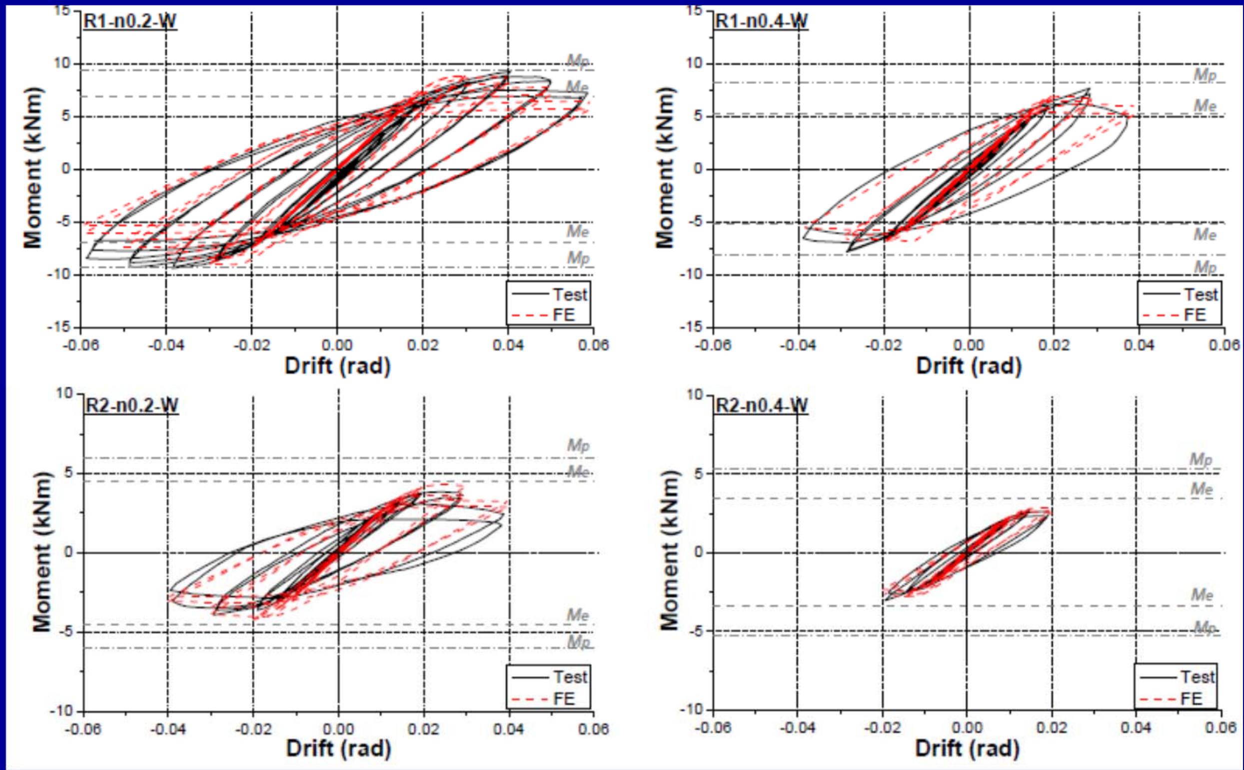


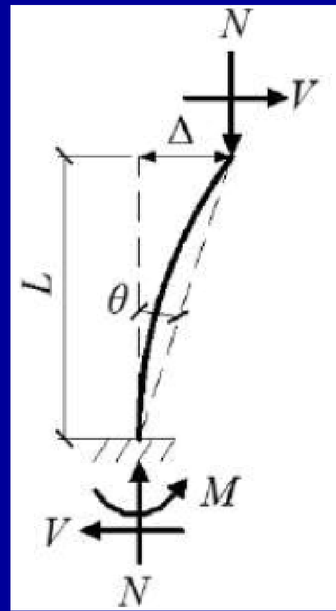


Moment, $M = VL + N\Delta$

Drift, $\theta = VL + N\Delta$

- **A much more compact behavior was found by specimens S1-n0.2, R1-n0.2-S, and R1-n0.4-S with less slender sections, where Mp can be achieved but with limited deformability. It is worthy noted that, according to the codified classification limits, the specimens are all class 4 sections with the exception of specimen R1-n0.2-S which belongs to class 3 section.**

# Experimental study—Skeleton curves

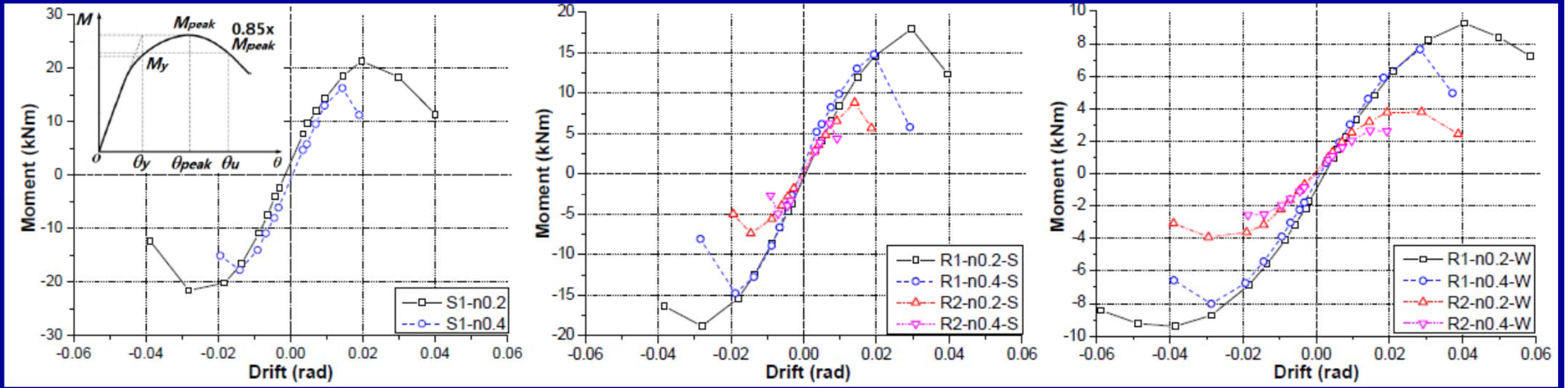


- The specimens exhibit low to moderate levels of ductility
- the highest □ is 2.60 for specimen R1-n0.2-W.

| Specimens | $M_u$(kNm) | $M_u/M_p$ | $M_u/M_e$ | $\theta_y$ (%) | $\theta_u$ (%) | $\mu$ |
|---|---|---|---|---|---|---|
| S1-n0.2 | 21.44 | 1.04 | 1.44 | 1.40 | 3.10 | 2.22 |
| S1-n0.4 | 17.02 | 0.94 | 1.52 | 1.06 | 1.80 | 1.69 |
| R1-n0.2-S | 18.38 | 1.22 | 1.80 | 1.84 | 3.72 | 2.02 |
| R1-n0.4-S | 14.77 | 1.12 | 1.93 | 1.27 | 2.18 | 1.72 |
| R2-n0.2-S | 8.10 | 0.83 | 1.22 | 1.01 | 1.64 | 1.64 |
| R2-n0.4-S | 5.63 | 0.66 | 1.13 | 0.62 | 0.79 | 1.30 |
| R1-n0.2-W | 9.33 | 1.00 | 1.35 | 2.27 | 5.91 | 2.60 |
| R1-n0.4-W | 7.83 | 0.96 | 1.51 | 1.91 | 3.47 | 1.81 |
| R2-n0.2-W | 3.86 | 0.64 | 0.85 | 1.49 | 3.45 | 2.31 |
| R2-n0.4-W | 2.62 | 0.50 | 0.77 | 1.02 | 1.87 | 1.84 |

- The lowest □ (i.e., 1.30) is observed in specimen R2-n0.4-S which has a slender section and is subjected to a high axial load ratio.

# Experimental study—Ductility

- Alternatively, the ductility or deformability characteristics of steel members can be directly assessed by $\theta_u$
- Under an axial load ratio of 0.2, most of the specimens can satisfy the criterion of DCM or IMF, except for specimen R2-n0.2-S.
- Minor-axis bending could often lead to increased $\theta_u$ due to increased member flexibility, and it is noticed that specimen R1-n0.2-W could well achieve the criterion of SMF.
- When the axial load ratio increases to 0.4, a large number of the specimens fail to meet the IMF criterion.

| | | |
|---|---|---|
| Eurocode 8 | ductility class medium (DCM) | ductility class high (DCH) |
| | $\theta u > 0.025$ | $\theta u > 0.035$ |
| AISC | intermediate moment frame (IMF) | special moment frame (SMF) |
| | $\theta u > 0.02$ | $\theta u > 0.04$ |

| Specimens | $M_u$(kNm) | $M_u/M_p$ | $M_u/M_e$ | $\theta_y$ (%) | $\theta_u$ (%) | $\mu$ |
|---|---|---|---|---|---|---|
| S1-n0.2 | 21.44 | 1.04 | 1.44 | 1.40 | 3.10 | 2.22 |
| S1-n0.4 | 17.02 | 0.94 | 1.52 | 1.06 | 1.80 | 1.69 |
| R1-n0.2-S | 18.38 | 1.22 | 1.80 | 1.84 | 3.72 | 2.02 |
| R1-n0.4-S | 14.77 | 1.12 | 1.93 | 1.27 | 2.18 | 1.72 |
| R2-n0.2-S | 8.10 | 0.83 | 1.22 | 1.01 | 1.64 | 1.64 |
| R2-n0.4-S | 5.63 | 0.66 | 1.13 | 0.62 | 0.79 | 1.30 |
| R1-n0.2-W | 9.33 | 1.00 | 1.35 | 2.27 | 5.91 | 2.60 |
| R1-n0.4-W | 7.83 | 0.96 | 1.51 | 1.91 | 3.47 | 1.81 |
| R2-n0.2-W | 3.86 | 0.64 | 0.85 | 1.49 | 3.45 | 2.31 |
| R2-n0.4-W | 2.62 | 0.50 | 0.77 | 1.02 | 1.87 | 1.84 |

- This suggests that the current specimens, especially those with slender sections, may not be suitable for seismic active regions unless a suitably low level of design load ratio is maintained.

# Experimental study—Energy dissipation

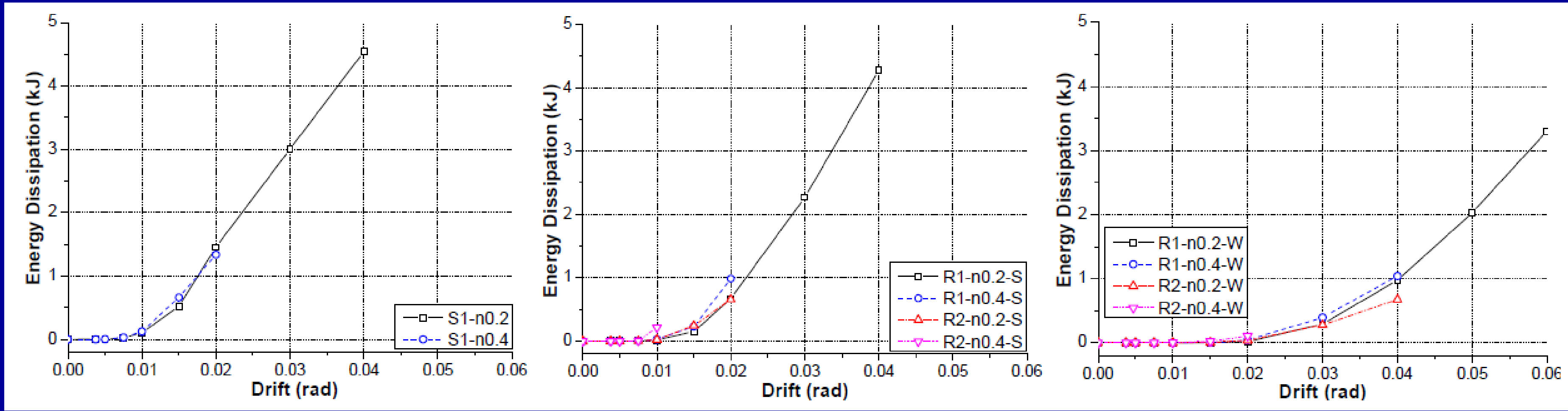


- **It is found that the specimens with the same section type but under different axial load ratios follow a similar increasing trend of energy dissipation, but the final $E_{total}$ differs significantly as ductility can be compromised by the increase of the load ratio.**
- **The energy dissipation capacity of the specimen with a more slender section is significantly suppressed due to early local buckling.**

# Numerical Investigation—FEM

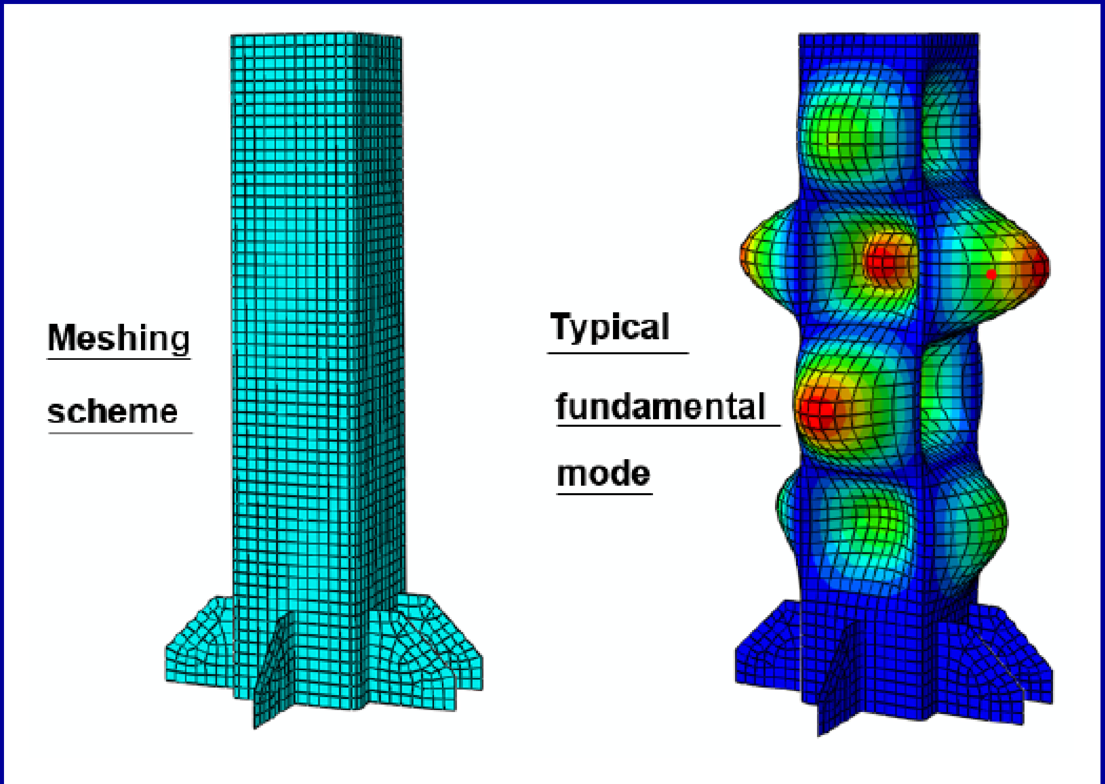


- the FE model was discretized by S4R elements with a meshing size of approximately 10 mm.
- the corner parts of the tube were carefully modelled.
- the initial local geometric imperfection was considered for the FE models.

# Numerical Investigation—FEM Verification

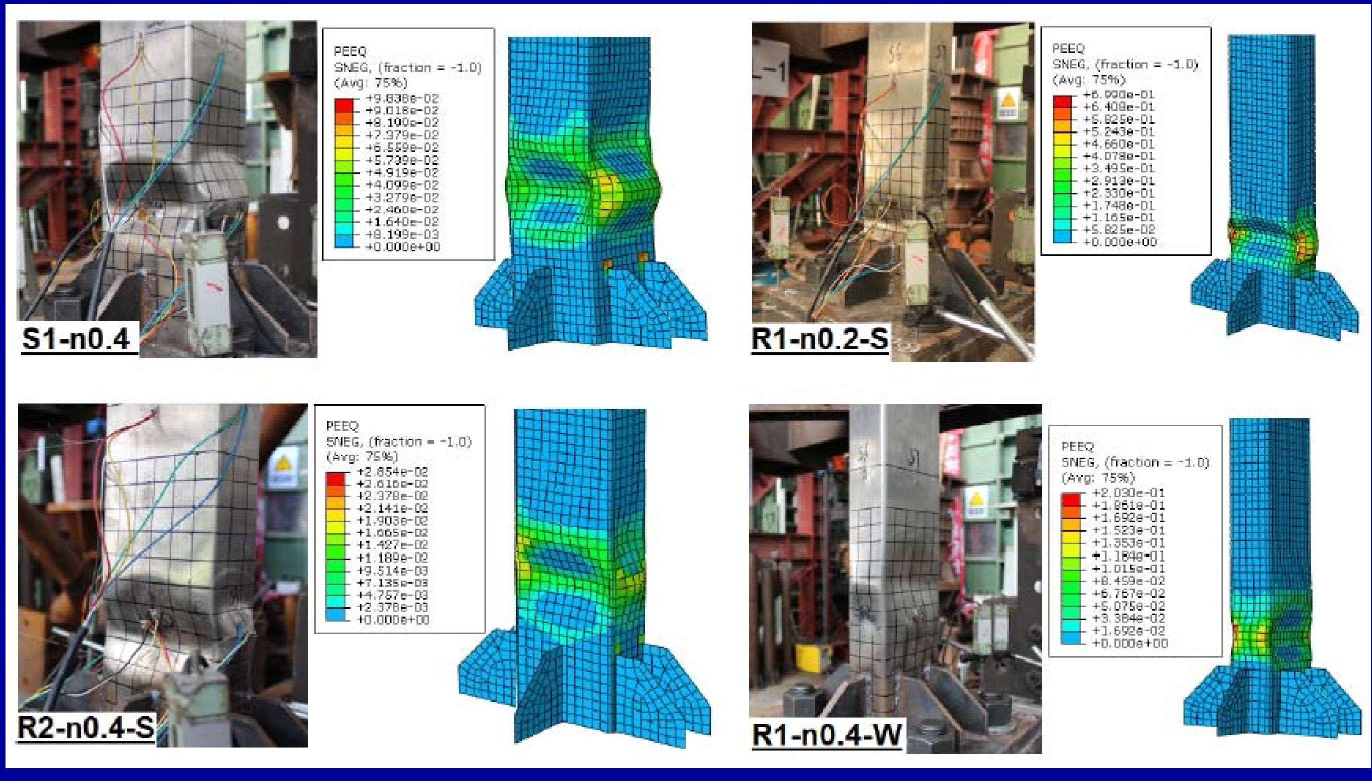


**Agree well**

| | *Test results* | | | | | | *FE predictions* | | | | | |
|---|---|---|---|---|---|---|---|---|---|---|---|---|
| Specimens | $M_u$(kNm) | $M_u/M_p$ | $M_u/M_e$ | $\theta_y$ (%) | $\theta_u$ (%) | $\mu$ | $M_{u\text{-}FE}$ (kNm) | $M_u/M_{u\text{-}FE}$ | $\theta_{y\text{-}FE}$ (%) | $\theta_y/\theta_{y\text{-}FE}$ | $\theta_{u\text{-}FE}$ (%) | $\theta_u/\theta_{u\text{-}FE}$ |
| S1-n0.2 | 21.44 | 1.04 | 1.44 | 1.40 | 3.10 | 2.22 | 20.83 | 1.03 | 1.14 | 1.23 | 2.26 | 1.37 |
| S1-n0.4 | 17.02 | 0.94 | 1.52 | 1.06 | 1.80 | 1.69 | 16.96 | 1.00 | 0.94 | 1.13 | 1.53 | 1.18 |
| R1-n0.2-S | 18.38 | 1.22 | 1.80 | 1.84 | 3.72 | 2.02 | 19.11 | 0.96 | 1.63 | 1.13 | 3.24 | 1.15 |
| R1-n0.4-S | 14.77 | 1.12 | 1.93 | 1.27 | 2.18 | 1.72 | 15.51 | 0.95 | 1.33 | 0.96 | 1.85 | 1.18 |
| R2-n0.2-S | 8.10 | 0.83 | 1.22 | 1.01 | 1.64 | 1.64 | 9.49 | 0.85 | 1.15 | 0.88 | 1.73 | 0.95 |
| R2-n0.4-S | 5.63 | 0.66 | 1.13 | 0.62 | 0.79 | 1.30 | 6.15 | 0.91 | 0.75 | 0.82 | 0.89 | 0.89 |
| R1-n0.2-W | 9.33 | 1.00 | 1.35 | 2.27 | 5.91 | 2.60 | 8.93 | 1.05 | 2.35 | 0.97 | 4.96 | 1.19 |
| R1-n0.4-W | 7.83 | 0.96 | 1.51 | 1.91 | 3.47 | 1.81 | 6.87 | 1.14 | 1.84 | 1.04 | 3.81 | 0.91 |
| R2-n0.2-W | 3.86 | 0.64 | 0.85 | 1.49 | 3.45 | 2.31 | 4.22 | 0.92 | 1.57 | 0.95 | 3.49 | 0.99 |
| R2-n0.4-W | 2.62 | 0.50 | 0.77 | 1.02 | 1.87 | 1.84 | 2.81 | 0.93 | 1.06 | 0.96 | 2.00 | 0.94 |
| Mean | | | | | | | | **0.97** | | **1.01** | | **1.07** |
| CoV | | | | | | | | **0.079** | | **0.118** | | **0.151** |

# Numerical Investigation—Parametric study

- A further parametric study was carried out to examine the influence of an extended range of parameters on the cyclic behavior of stainless steel RHSs/SHSs.

| Parameters | Details |
|---|---|
| Axial load ratio | 0.2, 0.4, 0.6 |
| Tube wall thickness (mm) | 3, 4, 6, 8, 10 |
| Section type (mm) | 180×90, 180×120, 180×150, 180×180 |
| Bending direction (for RHSs) | Major-axis, Minor-axis |
| Total number of model | 105 |

- width-to-thickness ratios ranging from 5.7 to 78.2;
- both strong-axis and weak-axis bending scenarios were considered;
- three practical levels of load ratio were taken into account, i.e. n = 0.2, 0.4, and 0.6.

# Design—Strength

- the FE-to-design predicted ratios for the design rules are above unity, indicating that the current design predictions are conservative.
- the design predictions could be unsafe for slender sections under combined high axial load ratios and cyclic bending.

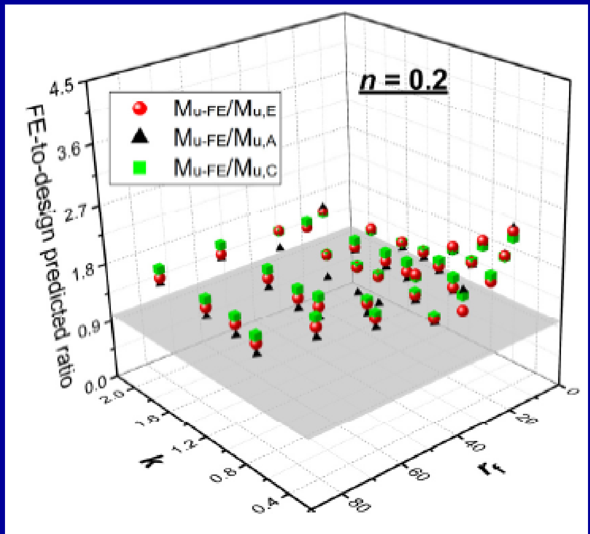


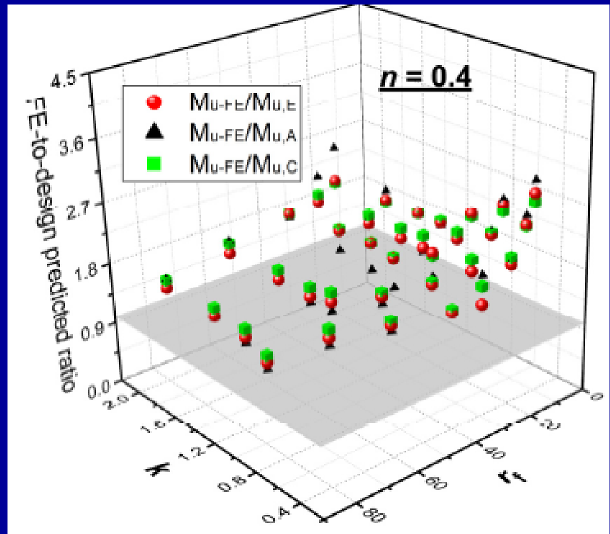


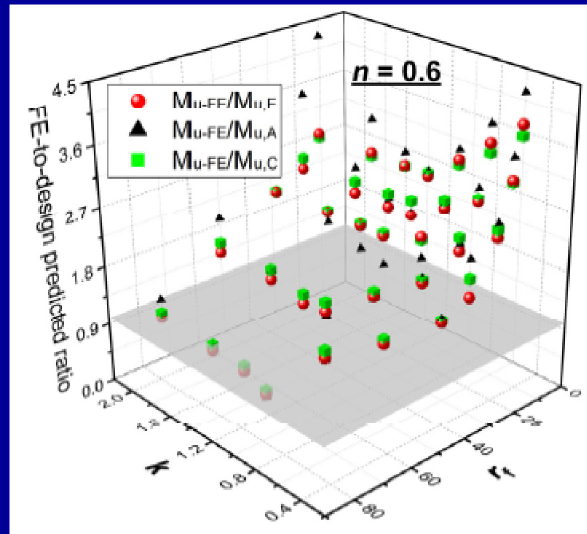


$$\frac{N_{\mathrm{Ed}}}{(N_{\mathrm{b,Rd}})_{\min}} + k_{\mathrm{y}}\left(\frac{M_{\mathrm{y,Ed}} + N_{\mathrm{Ed}}e_{\mathrm{Ny}}}{\beta_{\mathrm{W,y}}W_{\mathrm{pl,y}}f_{\mathrm{y}}/\gamma_{\mathrm{M1}}}\right) \le 1$$

Euro code 3）

$$\begin{cases} \dfrac{P_{\mathrm{u}}}{\phi_{\mathrm{c}}P_{\mathrm{n}}} + \dfrac{C_{\mathrm{my}}M_{\mathrm{uy}}}{\phi_{\mathrm{b}}M_{\mathrm{ny}}\alpha_{\mathrm{ny}}} \le 1.0 & \dfrac{P_{\mathrm{u}}}{\phi_{\mathrm{c}}P_{\mathrm{n}}} > 0.15 \\ \dfrac{P_{\mathrm{u}}}{\phi_{\mathrm{c}}P_{\mathrm{n}}} + \dfrac{M_{\mathrm{uy}}}{\phi_{\mathrm{b}}M_{\mathrm{ny}}} \le 1.0 & \dfrac{P_{\mathrm{u}}}{\phi_{\mathrm{c}}P_{\mathrm{n}}} \le 0.15 \end{cases}$$

SEI/ASCE 8-02）

$$\frac{N}{\varphi A_{\mathrm{e}}} + \frac{\beta_{\mathrm{m}}M}{(1-\varphi\dfrac{N}{N'_{\mathrm{E}}})W_{\mathrm{e}}} \le f$$

Chinese code ）

# Design—Ductility

- A ductility base design is proposed in order to offer a reliable evaluation for predicting the available ductility supply of stainless steel RHSs/SHSs.
- Employing the proposed equation, the section deformability of a stainless steel column under earthquake excitations can be reasonably assessed.

$$\theta_u = \frac{Z_0 + A_{01}k + B_{01}r_f + B_{02}r_f^2 + B_{03}r_f^3}{1 + A_1 k + A_2 k^2 + A_3 k^3 + B_1 r_f + B_2 r_f^2}$$

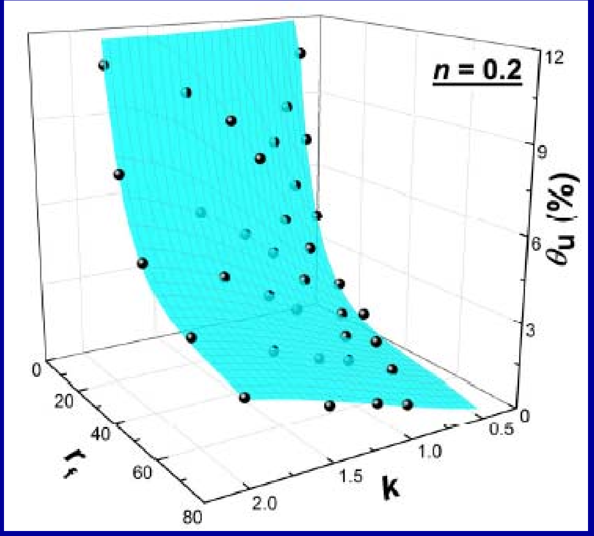


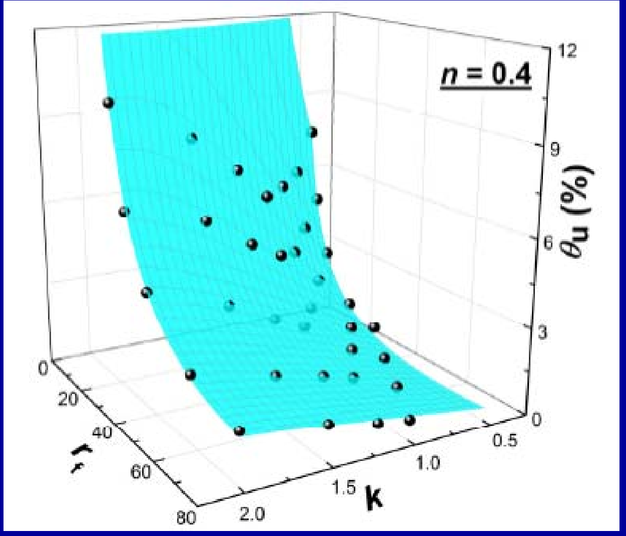


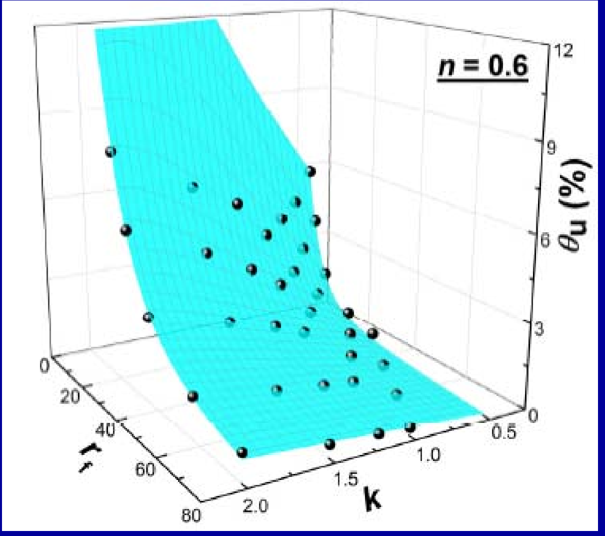

# Conclusions

- The behaviour of stainless steel rectangular and square hollow sections (RHSs and SHSs) under combined compression and uniaxial cyclic bending has been discussed in this study.
- The failure mode of all the test specimens is governed by local buckling. Moreover, RHSs under strong-axis bending experiences earlier local buckling compared with those under weak-axis bending.
- Most of the specimens are classified as class 4 sections according to Eurocode 3, but in fact, they could well achieve their elastic moment resistance Me. This indicates that the current codified classification limits are conservative.

# Conclusions

- The specimens exhibit low to moderate levels of ductility. According to AISC, the specimens can generally satisfy the criterion of IMF (and possibly SMF), provided that a low axial load ratio (i.e., n = 0.2) is applied. When the axial load ratio increases to 0.4, the specimens can hardly meet the IMF criterion. The results suggest that the current specimens may not be suitable for seismic active regions unless a sufficiently low design load ratio is ensured.
- From an energy dissipation point of view, strong-axis bending can lead to more energy dissipation compared with the case of weak-axis bending. Increasing the axial load ratio or section slenderness could compromise the energy dissipation capacity of the specimens due to decreased ductility.

# Conclusions

- The parametric study results show that the major design codes provide conservative predictions in terms of the strength of stainless steel beam-columns; the conservatism may be related to inaccurate considerations of constituent plate element interaction, nonlinear stress-strain response of stainless steel, and enhanced strength of the corner parts.
- A ductility base design is proposed to offer a reliable evaluation for predicting the available ductility supply of stainless steel RHSs/SHSs under different loading conditions.

# Thank you

**Tongji University** 同濟大學土木工程學院

**The 8th International conference on**

# Thin-walled Structures

**July 24-27, 2018**

**Lisbon, Portugal**

**Conference co-chair:**

**D. Camotim**

**N. Silvestre**